Results in Physics 43 (2022) 106132

Contents lists available at ScienceDirect

Results in Physics

journal homepage: www.elsevier.com/locate/rinp

First-principles calculations to investigate structural, elastic, electronic and thermodynamic properties of NbCoSn and VRhSn Half-Heusler compounds

Job W. Wafula [a,*], John W. Makokha [a], George S. Manyali [b]

[a] Department of Science, Technology and Engineering, Kibabii University, 1699-50200, Bungoma, Kenya
[b] Computational and Theoretical Physics (CTheP) Group, Department of Physical Sciences, Kaimosi Friends University, 385-50309, Kaimosi, Kenya

ARTICLE INFO

Keywords:
First-principles
Half-Heusler
NbCoSn
VRhSn

ABSTRACT

In this study, we investigated the structural, elastic, electronic, and thermodynamic properties of NbCoSn and VRhSn HH compounds using the first-principles calculations as implemented in the density functional theory (DFT). The computed lattice constants of NbCoSn and VRhSn compounds were found to be consistent with the available theoretical as well as the experimental data. The compounds are mechanically stable since their elastic constants satisfy the Born-Huang criteria for cubic system stability. Due to the absence of imaginary phonons, NbCoSn is dynamically stable, whereas VRhSn is unstable. NbCoSn is harder than VRhSn HH because it has a higher Vicker's hardness and shear modulus. Both compounds feature band gaps, indicating that they are semiconductors. When compared to NbCoSn HH compound, VRhSn has a narrow band gap. Furthermore, thermodynamic properties are computed and thoroughly explored. As a result of the findings, NbCoSn and VRhSn HH compounds are viable thermoelectric materials; however, doping and alloying could be employed to enhance the stability of VRhSn HH compound.

Introduction

Half-Heusler compounds are XYZ compounds that crystallize in a cubic structure (F43m, C_{1b}, space group no. 216). HH compounds with 8 valence electrons are semiconductors having a broad energy interval in their bandgap. In general, compounds of the I-II-V, I-III-IV, II-II-IV, and III-II-III type combinations are half-Heusler materials with eight valence electrons [1–3].

Since energy generation based on TE offers a potential answer to the twenty-first-century energy dilemma due to the fact that this method does not rely on fossil fuels and is thus ecologically benign, HH compounds have become materials of interest in the thermoelectric industry since thermoelectric materials are used in thermoelectric generators to convert heat to electricity and vice versa [4,5]. Aside from producing electrical energy, thermoelectrics technology also minimize thermal pollution caused by the presence of surplus heat in the environment. The effectiveness of energy conversion is greatly dependent on the type of thermoelectric materials utilized. Because of their low band gaps, most Half-Heusler (HH) compounds are ideal for thermoelectric materials intended for TEG [6–8]. However, one of the HH compounds' problems is thermal and mechanical compatibility.

Previous research has shown that the NbCoSn HH compound is mechanically stable, and it has been proposed for use as a thermoelectric material as well as for optoelectronic purposes [9]. Its thermodynamic stability, however, was not explored.

Despite the fact that the VRhSn compound has a lesser possibility of developing a half-Heusler (HH) structure, it has been identified as an attractive option to examine [10]. Furthermore, at a high temperature of roughly 700 K, the VRhSn HH compound is found to have a comparatively low lattice thermal conductivity of 7.11 W/mK [11]. As a result, the current work was motivated by a desire to better understand the mechanical and thermal properties of the VRhSn HH compounds.

The aim of this study was to investigate the structural, elastic, electronic, and thermodynamic properties of NbCoSn and VRhSn HH compounds using density functional theory (DFT) as implemented in the quantum ESPRESSO code. The computational details of this work are explained in section II. Section III consists of the results and discussions, while Section IV contains the conclusion.

Computational details

Based on density functional theory, the structural, mechanical,

* Corresponding author.
E-mail address: jobwafula691@gmail.com (J.W. Wafula).

https://doi.org/10.1016/j.rinp.2022.106132
Received 22 September 2022; Received in revised form 10 November 2022; Accepted 23 November 2022
Available online 24 November 2022

electronic, and thermodynamic properties of NbCoSn and VRhSn were examined in this work. Interactions between core and valence electrons were studied using Quantum Espresso Pslibrary 1.0.0 projector augmented wave (PAW) pseudo-potentials [12]. Perdew-Burke-Ernzerhof (PBE) with generalized gradient approximations (GGA) and local density approximation (LDA) were used to calculate the exchange–correlation energies [13,14]. The plane wave cu-toff energies for NbCoSn and VRhSn were set at 120 Ry for both the materials. For elastic properties of NbCoSn and VRhSn HH compounds, the Monkhorst-Pack special k-point system [15] with 8 × 8 × 8 k-points in the Brillouin zone were utilized while dense k-points of 32 × 32 × 32 were used to compute DOS and band structures. The total energy (E_{tot}) as a function of the unit cell volume (V) was interpolated by the Murnaghan's equation of state [16] as indicated in equation (1) to determine the equilibrium lattice constants of NbCoSn and VRhSn compounds.

$$E(V) = E(V_0) + \frac{B_0}{B_0^{'} + (B_0^{'} - 1)}\left[V\left(\frac{V_0}{V}\right)B_0^{'} - V_0\right] + \frac{B_0}{B_0^{''}}(V - V_0) \quad (1)$$

where E(V) refers to the ground state energy with a volume of cell (V), V_0 is the volume of unit cell at zero pressure, B_0 and B_0 are modulus of compressibility and its derivative, respectively.

The thermo_pw algorithm computed elastic constants as well as other auxiliary elastic properties such bulk moduli, shear moduli, Young's moduli, and poison's ratios using elastic tensors using Voigt-Reuss-average. Hill's averages of bulk and shear moduli are used to compute sound velocities. The Debye temperature is derived using a precise method that takes the angular average of the sound velocities calculated for each propagation direction and solves the Christoffel wave equation. Within the Debye model, the accurate Debye temperature is employed to compute the vibrational energy, free energy, entropy, and constant strain heat capacity [17–19]. The phonon dispersions, at the equilibrium structures of NbCoSn and VRhSn compounds were computed based on the density functional perturbation theory (DFPT) as implemented in the thermo_pw code [17]. A 2 × 2 × 2 grid of q-points was utilized to obtain phonon frequencies, and Fourier interpolation was applied for other points in the BZ.

Results and discussions

Structural properties

The half-Heusler compounds NbCoSn and VRhSn have a C_{1b} cubic structure with the space group F43m (216). The unit cells of NbCoSn and VRhSn structures were optimized in terms of internal atomic locations and lattice parameters to get the equilibrium structures shown in Fig. 1 generated by the xcrysden programme [20]. The computed lattice parameters of NbCoSn and VRhSn HH compounds, 5.972 Å and 6.061 Å for GGA-PBE while 5.855 Å and 5.942 Å for LDA functionals respectively, correspond well with earlier theoretical and experimental data [9–10,21], as shown in Table 1, proving the study's credibility.

Elastic properties

Most of a compound's structural, thermal, and mechanical behaviors are determined by its elastic properties. Furthermore, elastic properties provide further information about how a particular material responds to external forces applied to the crystal. The three independent elastic constants of cubic crystals are C_{11}, C_{12} and C_{44} [22]. The thermo_pw code was used to calculate the elastic constants, and the strains were induced to the primitive vectors of the unstrained structures [17–18]. Elastic constants C_{11} and C_{12} are determined by the volume conserving tetragonal strain, while C_{44} can calculate by orthorhombic strain [23]. Table 1 displays larger values of elastic constants (C_{ij}) of NbCoSn and VRhSn for LDA compared to that obtained from GGA-PBE approximation since LDA overbinds the unit cell while PBE underbinds. According to the Born-Huang stability criterion for every cubic system, as provided by the equations $C_{11} > 0$, $C_{44} > 0$, C_{11}-$C_{12} > 0$, ($C_{11} + 2C_{12} > 0$ and $C_{12} < B > C_{12}$ [24], implying that NbCoSn and VRhSn crystals are mechanically stable. We noted that the elastic constants C_{11} are greater than C_{12} and C_{44}, indicating that more external force is required to compress the NbCoSn and VRhSn HH compounds along the a-axes than along the b- and c-axes. Furthermore, the lower resistance to shear deformation compared to resistance to unidirectional compression is due to the fact that the elastic constants C_{11} are bigger than C_{44} for instance the compounds studied. Other key mechanical parameters for polycrystalline materials, such as shear modulus (G) Young's modulus (E) and Poisson's ratio (v) are commonly evaluated and computed to examine their hardness [25]. They are derived from the estimated elastic constants by using the following equations ((2)–(8)) [26];

$$B = \frac{B_V + B_R}{2} \quad (2)$$

B denotes a material's capacity to withstand volume change. Equations (2) calculate the Voigt bulk modulus (B_V) and the Reuss bulk modulus (B_R).

$$B_V = B_R = \frac{C_{11} + 2C_{12}}{3} \quad (3)$$

$$G = \frac{G_V + G_R}{2} \quad (4)$$

G is the shear modulus, which influences the resistance to plastic

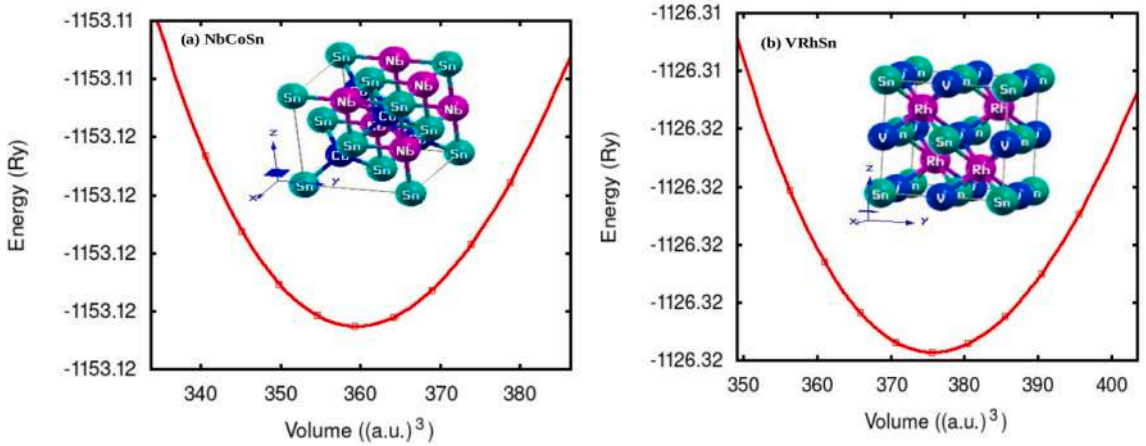

Fig. 1. (color online) Figures (a) and (b) indicates the structural properties of NbCoSn and VRhSn HH compounds respectively obtained from GGA-PBE functionals.

Table 1
Calculated ground state structural and elastic properties of NbCoSn and VRhSn HH compounds using GGA-PBE and LDA exchange correlation functionals.

	a(A)	C11 (GPa)	C12 (GPa)	C44 (GPa)	B (GPa)	G (GPa)	E (GPa)	v	A
NbCoSn	$_{5.972}GGA$	286.09	91.25	63.09	156.20	75.13	194.24	0.2926	0.647
	$_{5.855}LDA$	336.37	107.80	75.85	183.99	89.43	230.88	0.29078	0.663
	6.01 ^{GGA} [9]	282.04	105.23	64.49	164.17	73.18	191.15	0.3059	0.729
	5952^{E,}P^{f} [21]								
	6.061^{G,,}	204.99	118.90	36.93	147.60	39.26	108.20	0.3778	0.857
VRhSn	5.942^{LDA}	242.67	138.98	50.00	173.55	50.73	138.68	0.3668	0.964
	6.192^{GGA} [10]								

deformation. Equations (4) and (5) provide the Voigt shear modulus (G_V) and the Reuss shear modulus (G_R).

$$G_V = \frac{C_{11} - C_{12} + 3C_{44}}{5} \tag{5}$$

$$G_R = \frac{5(C_{11} - C_{12})C_{44}}{4C_{44} + 3(C_{11} - C_{12})} \tag{6}$$

$$E = \frac{(C_{11} - C_{12})(C_{11} + 2C_{12})}{C_{11} + C_{12}} \tag{7}$$

E stands for Young's modulus, which represents the stiffness of the material in relation to length change.

$$v = \frac{3B - 2G}{6B + 2G} \tag{8}$$

Table 1 shows the bulk moduli (B), shear moduli (G), and Young's moduli (E) of NbCoSn and VRhSn HH compounds determined from this investigation. Table 1 shows that the computed values of bulk moduli (B) of the NbCoSn compound are bigger than those of VRhSn, indicating that NbCoSn has a higher resistance to volume change as well as greater bond strength. It has been demonstrated that shear moduli, rather than bulk moduli, have a key role in forecasting material hardness [27]. Because the shear modulus of the NbCoSn HH compound is greater than that of VRhSn, NbCoSn is tougher than VRhSn.

Furthermore, using the empirical formula proposed by Chen-Niu model indicated in equation (9), we predicted the Vicker's hardness of NbCoSn and VRhSn HH compounds [28].

$$H_v = 2\left(\frac{G^3}{B^2}\right)^{0.585} - 3 \tag{9}$$

Based on the computed hardness values, we discovered that NbCoSn crystal is harder than VRhSn since its Vicker's hardness was 7.628 GPa (for GGA-PBE) and 8.914 GPa (for LDA) whereas VRhSn's was 0.635 GPa (for GGA-PBE) and 1.716 GPa (for LDA). Poison's ratio values for NbCoSn and VRhSn HH compounds are 0.2926 and 0.3778, respectively, and the ratios were >2/7, as shown in Table 1, showing that the materials studied in this investigation are ductile [29]. The elastic anisotropy factor $A = 2C_{44}/(C_{11}\text{-}C_{12})$ was determined, and if A = 1, the crystal is isotropic, but any value less or>1 shows anisotropy [30]. The anisotropy factors of NbCoSn and VRhSn HH compounds are provided in Table 1 and are less than one for both GGA-PBE and LDA exchange correlation functionals, indicating that the materials studied in this investigation are anisotropic.

To understand the resistance of the materials to stresses caused by bending or stretching forces, we determined the Kleinman parameter (ς) using equation (10); [31]

$$\varsigma = \frac{C_{11} + 8C_{12}}{7C_{11} + 2C_{12}} \tag{10}$$

The dimensionless Kleinman parameter typically has a value between $0 \leq \varsigma \leq 1$. The higher limit of the Kleinman parameter (ς) indicates the minor contribution of bond stretching to external stress resistance, whereas the lower limit corresponds to the insignificant contribution of bond bending to external stress resistance [32]. The values of the Kleinman parameter (ς) determined for NbCoSn and VRhSn compounds are 0.465 and 0.691 for GGA-PBE while 0.4664 and 0.6852 for LDA, respectively. This means that mechanical strength in NbCoSn is mostly determined by bond bending rather than bond stretching or contracting. When compared to bond bending, the mechanical strength of VRhSn is dominated by the bond stretching or contracting contribution.

Electronic properties

Both materials' phonon dispersion curves and phonon_DOS were estimated along the high symmetry points (Γ-X-K-Γ-L-W-X) of the Brillouin zone, as illustrated in Fig. 2 (a) and (b). Because there are no imaginary phonon frequencies, the NbCoSn compound is dynamically stable. The existence of imaginary phonon frequencies in the phonon spectra of the VRhSn compound, on the other hand, is unequivocal indication that it is dynamically unstable [33–37].

At the ground state conditions, the electronic energy band structures and total density of states of NbCoSn and VRhSn HH compounds were estimated along the high symmetry points (Γ-X-K-Γ-L-W-X) in the first BZ, as shown in Fig. 3 and Fig. 4 respectively. At Fermi level E_F (E = 0 eV), we detected an indirect band gap (Γ-X) between the valence band and the conduction band, confirming that NbCoSn and VRhSn HH compounds are semiconductors. The valence-band maximum (VBM) of NbCoSn is at the L and W points, whereas the conduction-band minimum (CBM) is at the X point. The valence-band maximum (VBM) of VRhSn, on the other hand, is located at Γ and W points, while the conduction-band minimum (CBM) is located at the X point [38]. Table 2 shows that the estimated band gaps of NbCoSn and VRhSn HH compounds were in good agreement with earlier experimental and theoretical research [9–10,39]. Furthermore, the VRhSn HH compound has a narrower band gap than the NbCoSn compound, indicating that VRhSn could be a promising thermoelectric material if its dynamical stability is improved. The distribution of the electronic states of a system as a function of energy is expressed as the density of states of a solid [40]. Fig. 5 and Fig. 6 indicates the spin-polarized total density of states (DOS) of NbCoSn and VRhSn compounds respectively. Each density of states curve has an upper section that represents the plot of spin majorities and a lower part that represents the plot of spin minorities [41]. The presence of symmetry in the two curves demonstrates that the two alloys are non-magnetic [42]. In addition, total magnetisation of both the compounds from spin-polarized calculations are 0.00 μB/f.u thus implying that the materials are non-magnetic.

Thermodynamic properties

The evaluation of thermodynamic properties under temperature offers critical information on chemical stability, which is required for the identification of these materials in order to utilize them effectively in the industrial sector [43,44]. Fig. 7 depicts the harmonic thermodynamic parameters of NbCoSn and VRhSn compounds at ground state conditions. Because a previous work by Benaddi *et al.* discovered that pressure has no effect on the changes of entropy and heat capacity with respect to temperature [45], the thermodynamic properties were calculated at zero pressure.

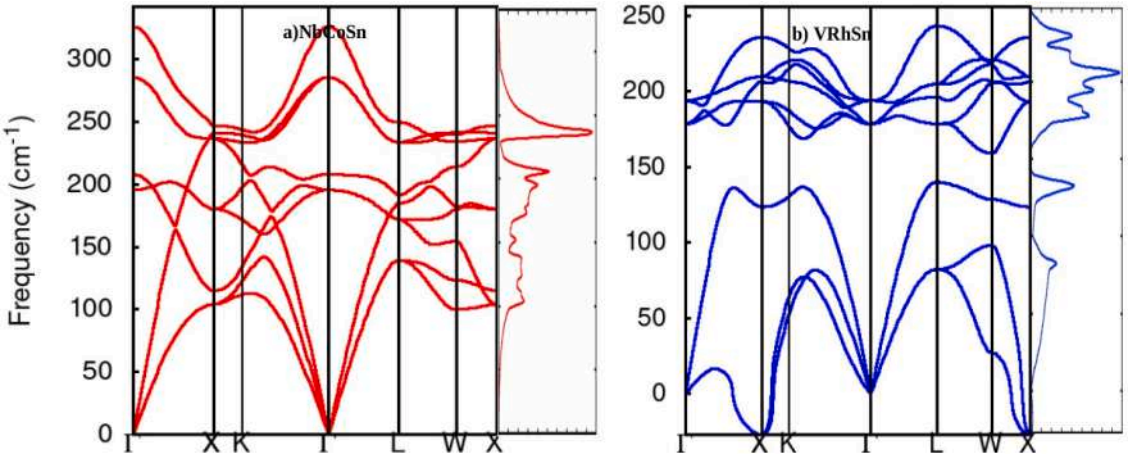

Fig. 2. (a) and (b) indicating the phonon dispersion curves and the phonon_DOS of NbCoSn and VRhSn HH compounds.

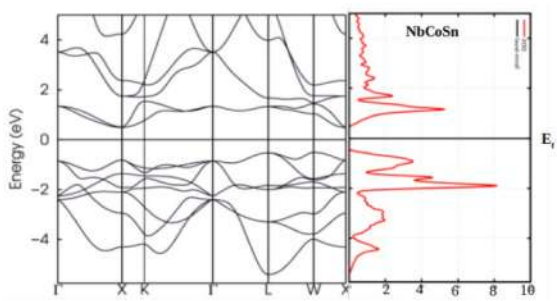

Fig. 3. Calculated electronic band structure and the density of states of NbCoSn HH compounds using GGA-PBE.

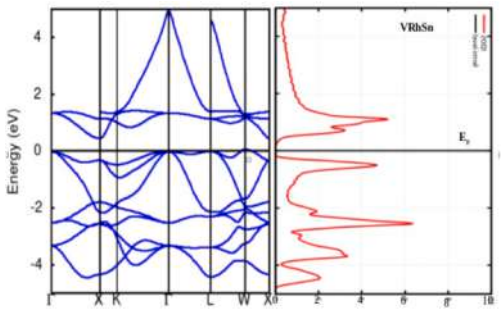

Fig. 4. Calculated electronic band structure and the density of states of VRhSn HH compounds using GGA-PBE.

Table 2
Calculated band gaps, debye temperatures (Θ_D), average sound velocities (v_m) and melting temperatures (T_m) for NbCoSn and VRhSn crystal structures respectively.

Compounds	XC	Band gap (eV)	(Θ_D) (K)	v_m (m/s)	$T_m \pm 300$ (*K*)
NbCoSn	GGA	0.997	378.59	3317.41	2243.79
	LDA	1.033	409.036	3512.99	2540.94
	GGA [9]	1.004			
	GGA + U [9]	0.958			
	GGA [39]	0.987			
	GGA	0.391	278.94	2479.33	1764.49
VRhSn	LDA	0.352	313.41	2732.24	1987.17
	GGA [10]	0.532			

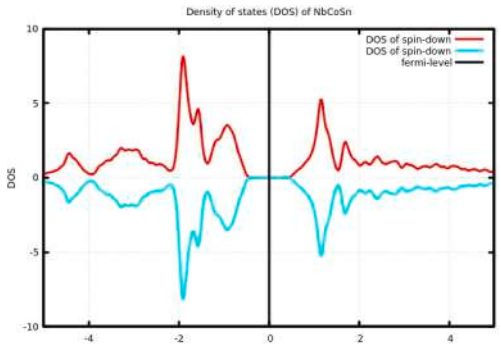

Fig. 5. Spin-polarized total density of states of NbCoSn HH compounds using GGA-PBE.

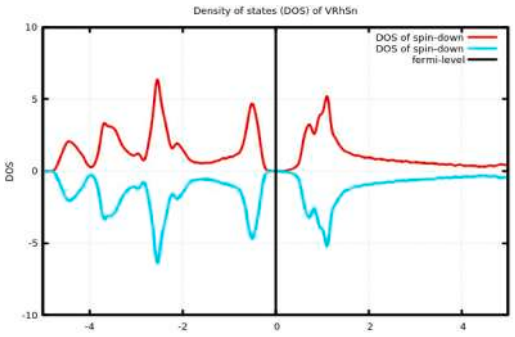

Fig. 6. Spin-polarized total density of states of VRhSn HH compounds using GGA-PBE.

The Debye vibrational energy for NbCoSn and VRhSn HH compounds remains constant below 100 K, while beyond 100 K, there are linear increase in vibrational energy with temperature, as seen in Fig. 7 (a). For temperatures beyond 100 K, however, vibrational free energy decreases because entropy (S) increases with temperature, as predicted by the equation F = U-TS [46], as illustrated in Fig. 7(b) and (c).

According to Fig. 7(c), the entropy of the VRhSn HH compound is greater than that of NbCoSn, indicating that the VRhSn system becomes more disordered as temperature increases when compared to NbCoSn.

For temperatures below 100 K, the values of entropy and heat capacity of NbCoSn and VRhSn compounds are essentially zero in Fig. 7(c) and (d). However, as temperatures rise above 100 K, entropy increases virtually linearly up to the greatest temperatures. At low temperatures

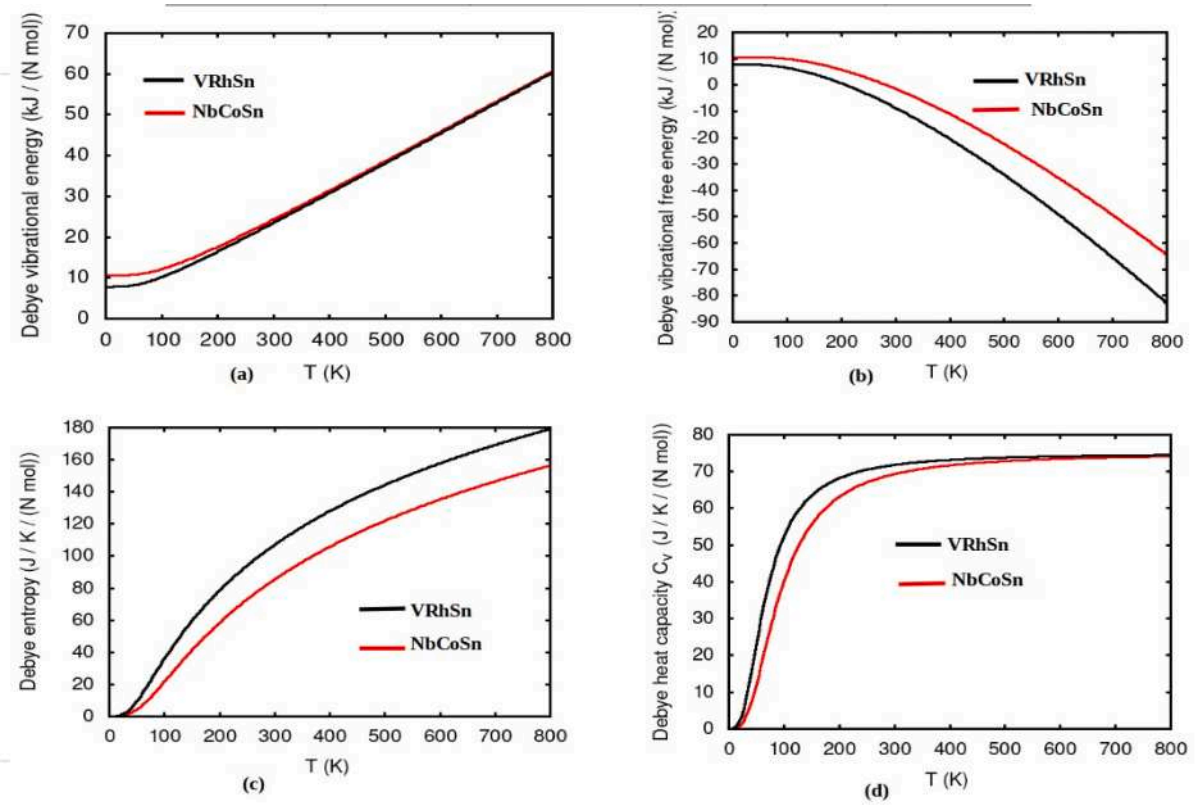

Fig. 7. (a, b, c and d) showing thermodynamic properties of NbCoSn and VRhSn HH compounds as a function of temperature obtained from GGA-PBE.

below 200 K, the heat capacity of NbCoSn and VRhSn HH compounds obeys the formula $C = AT^3$ due to anharmonic approximations, which corresponds to the lattice contribution to heat capacity. It is also worth noting that at high temperatures of 500 K and above, the heat capacity C_v is temperature independent demonstrating that the anharmonic effect on heat capacity is neglected and its value tends to the Dulong-Petit limit [47].

The Debye temperature (Θ_D) is a critical thermophysical parameter that describes the temperature at which all phonon modes are excited. As a result, it is closely related to thermophysical properties including heat capacity, thermal expansion, the Gruneisen parameter, and melting point. The Debye temperature value may be determined from the average sound wave velocities as illustrated by the equations ((11)–(14)); [48–51]

$$\Theta_D = \frac{h}{k_B}\left[\frac{3n}{4\pi}\left(\frac{N_A\rho}{M}\right)\right]^{\frac{1}{3}} v_m \tag{11}$$

where h denotes Planck's constant, k_B represents Boltzmann's constant, N_A refers Avogadro's number, ρ is the density, M is molecular weight, n is the number of atoms in the molecule, and v_m is the averaged wave velocity summed across several crystal directions,

$$v_m = \left[\frac{1}{3}\left(\frac{2}{v_t^3} + \frac{1}{v_l^3}\right)\right]^{-\frac{1}{3}} \tag{12}$$

where v_t and v_l are the transverse and longitudinal sound velocity calculated from the shear modulus (G) and bulk modulus (B) applying Navier's equation:

$$v_t = \left(\frac{B + \frac{4G}{3}}{\rho}\right)^{\frac{1}{2}} \tag{13}$$

$$v_l = \left(\frac{G}{\rho}\right)^{\frac{1}{2}} \tag{14}$$

It has been proven that the higher the Debye temperature, the greater the thermal conductivity, and vice versa. Minimum thermal conductivity (k_{min}), on the other hand, is exactly proportional to average sound velocity in crystals, as given by equation (11) [52];

$$k_{min} = k_B v_m \frac{nN_A\rho}{M} \tag{15}$$

Table 2 summarizes the Debye temperature and average sound velocity of NbCoSn and VRhSn compounds. VRhSn HH compound has lower Debye temperature and average sound velocity values, indicating that VRhSn has reduced thermal conductivity and might be a viable thermoelectric material.

Melting temperature

The empirical formula defined by equation (12) [53] was applied to predict the melting temperatures (T_m) of cubic crystals given elastic constant data.

$$T_m = [553K + (5.91K/GPa)C_{11}] \pm 300K \tag{16}$$

Table 2 lists the predicted melting temperatures of NbCoSn and VRhSn compounds. The high melting temperatures show that the compounds in this work, particularly the NbCoSn HH compounds, are suited for high-temperature applications.

Conclusion

The structural, elastic, electronic, and thermodynamic characteristics of NbCoSn and VRhSn HH compounds were determined using first-principles computations. The predicted ground state lattice parameters in this study were found to agree well with previous theoretical and

experimental data, indicating that the current study is reliable. The NbCoSn HH compound is both mechanically and dynamically stable, whereas VRhSn is mechanically stable but dynamically unstable. NbCoSn was found to be tougher than VRhSn material because it has a higher Vicker's hardness than VRhSn HH. Furthermore, the presence of the band gap at the femi level indicated that the compounds in this investigation are semiconductors. Finally, while both materials are acceptable for thermoelectric applications, doping or alloying or nano-structuring can be employed to increase the VRhSn HH compound's stability.

Author contributions

J.W.W, J.W.M and G.S.M conceptualized the study, acquired the data, did analysis and interpretation of data. J.W.W drafted the original article and revised it critically for important intellectual content. Final all authors approved the version to be submitted.

Declaration of Competing Interest

The authors declare that they have no known competing financial interests or personal relationships that could have appeared to influence the work reported in this paper.

Data availability

Data will be made available on request.

Acknowledgment

The authors express gratitude for a computational resource supplied by the Center for High-Performance Computing (CHPC) located at Cape Town, South Africa. Second, we thank Kibabii University's Department of Science, Technology, and Engineering for providing access to the internet, which allowed us to access the CHPC.

References

[1] Saim A, Belkharroubi F, Boufadi FZ, Ameri I, Blaha LF, Tebboune A, et al. Investigation of the structural, elastic, electronic, and optical properties of half-heusler CaMgZ (Z= C, Si, Ge, Sn, Pb) compounds. J Electron Mater 2022;51(7):4014–28.
[2] Gruhn T. Comparative ab initio study of half-Heusler compounds for optoelectronic applications. Phys Rev B 2010;82(12):125210.
[3] Gaid FO, BoufAdi FZ, Tayebi N, Ameri M, Mentefa A, Bellagoun L, et al. Theoretical investigation of structural, electronic, elastic, magnetic, thermodynamic, and thermoelectric properties of Ru2MnNb Heusler alloy: FP-LMTO method. Emergent Materials 2022;5(4):1065–73.
[4] Haque E, Hossain MA. First-principles study of elastic, electronic, thermodynamic, and thermoelectric transport properties of TaCoSn. Results Phys 2018;10:458–65.
[5] Mori T, Priya S. Materials for energy harvesting: At the forefront of a new wave. MRS Bull 2018;43(3):176–80.
[6] Yanagi K, Kanda S, Oshima Y, Kitamura Y, Kawai H, Yamamoto T, et al. Tuning of the thermoelectric properties of one-dimensional material networks by electric double layer techniques using ionic liquids. Nano Lett 2014;14(11):6437–42.
[7] Zhou W, Fan Q, Zhang Q, Cai L, Li K, Gu X, et al. High-performance and compact-designed flexible thermoelectric modules enabled by a reticulate carbon nanotube architecture. Nat Commun 2017;8(1):1–9.
[8] Caballero-Calero O, Ares JR, Martín-Gonzalez, M. Environmentally friendly thermoelectric materials: high performance from inorganic components with low toxicity and abundance in the earth. Adv. Sustain. Syst. 2021;5(11):2100095.
[9] Zerrouki T, Rached H, Rached D, Caid M, Cheref O, Rabah M. First-principles calculations to investigate structural stabilities, mechanical and optoelectronic properties of NbCoSn and NbFeSb half-Heusler compounds. Int J Quantum Chem 2021;121(8):e26582.
[10] Gzyl AS, Oliynyk AO, Mar A. Half-heusler structures with full-heusler counterparts: machine-learning predictions and experimental validation. Cryst Growth Des 2020;20(10):6469–77.
[11] Tranas R, Løvvik OM, Tomic O, Berland K. Lattice thermal conductivity of half-Heuslers with density functional theory and machine learning: enhancing predictivity by active sampling with principal component analysis. Comput Mater Sci 2022;202:110938.
[12] Giannozzi P, Andreussi O, Brumme T, Oana Bunau M, Nardelli B, Calandra M, et al. Advanced capabilities for materials modelling with Quantum ESPRESSO. J Phys Condens Matter 2017;29(46):465901.
[13] Perdew JP, Burke K, Ernzerhof M. Generalized gradient approximation made simple. Phys Rev Lett 1996;77:3865.
[14] Perdew JP, Wang Y. Accurate and simple analytic representation of the electron-gas correlation energy. Phys Rev B 1992;45(23):13244.
[15] Monkhorst HJ, Pack JD. Special points for Brillouinzone integrations. Phys Rev B 1976;13(12):5188.
[16] Murnaghan FD. The compressibility of media under extreme pressures. Proc Natl Acad Sci 1944;30(9):244–7.
[17] *http : //qeforge.qe − forge.org/gf/project/thermo$_p$w/.*
[18] Dal Corso A. Elastic constants of beryllium: a first-principles investigation. J Phys Condens Matter 2016;28:075401.
[19] Palumbo M, Dal Corso A. Lattice dynamics and thermophysical properties of hcp Os and Ru from the quasi-harmonic approximation. J Phys Condens Matter 2017;29(39):395401.
[20] Kokalj A. Computer graphics and graphical user interfaces as tools in simulations of matter at the atomic scale. Comp. Mater. Sci. 2003;28:155.
[21] Ferluccio DA, Smith RI, Buckman J, Bos JWG. Impact of Nb vacancies and p-type doping of the NbCoSn–NbCoSb half-Heusler thermoelectrics. PCCP 2018;20(6):39793987.
[22] Jamal M, Asadabadi SJ, Ahmad I, Aliabad HR. Elastic constants of cubic crystals. Comput Mater Sci 2014;95:592–9.
[23] Aouimer S, Ameri M, Bensaid D, Moulay NE, Bouyakoub AZ, Boufadi FZ, et al. The elastic, electronic and thermodynamic properties of a new Cd based full heusler compounds–A theoretical investigation using DFT based FP-LMTO approach. Acta Phys Pol A 2019;136(1).
[24] Li Y, Gao Y, Xiao B, Min T, Fan Z, Ma S, et al. Theoretical study on the stability, elasticity, hardness and electronic structures of W-C binary compounds. J Alloy Compd 2010;502(1):28–37.
[25] Khelfaoui F, Ameri M, Bensaid D, Ameri I, Al-Douri Y. Structural, elastic, thermodynamic, electronic, and magnetic investigations of full-Heusler compound Ag2CeAl: FP-LAPW method. J Supercond Nov Magn 2018;31(10):3183–92.
[26] Hill R. The elastic behaviour of a crystalline aggregate. Proc Phys Soc London, Sect A 1952;65:349.
[27] Kittel, C., 2021. Introduction to solid state physics Eighth edition.
[28] Chen X-Q, Niu H, Li D, Li Y. Modeling hardness of polycrystalline materials and bulk metallic glasses. Intermetallics 2011;19:1275–81.
[29] Greaves GN, Greer AL, Lakes RS, Rouxel T. Poisson's ratio and modern materials. Nat Mater 2011;10(11):823–37.
[30] Gueddouh A, Bentria B, Lefkaier IK. First-principle investigations of structure, elastic and bond hardness of FexB (x= 1, 2, 3) under pressure. J Magn Magn Mater 2016;406:192–9.
[31] Kleinman L. Deformation potentials in silicon. I. Uniaxial strain. Phys Rev 1962;128(6):2614.
[32] Naher MI, Naqib SH. Structural, elastic, electronic, bonding, and optical properties of topological CaSn3 semimetal. J Alloy Compd 2020;829:154509.
[33] Togo A, Tanaka I. First principles phonon calculations in materials science. Scripta Materialia 2015; 108: 1-5. 62.
[34] Yang T, Xie C, Chen H, Wang X, Zhang G. Phononic nodal points with quadratic dispersion and multifold degeneracy in the cubic compound Ta 3 Sn. Phys Rev B 2022;105(9):094310.
[35] Ding G, Zhou F, Zhang Z, Yu ZM, Wang X. Chargetwo Weyl phonons with type-III dispersion. Phys Rev B 2022;105(13):134303.
[36] Zhong M, Han Y, Wang J, Liu Y, Wang X, Zhang G. Material realization of double-Weyl phonons and phononic doublehelicoid surface arcs with P 2 1 3 space group. Phys Rev Mater 2022;6(8):084201.
[37] Zhou L, Han W. Driving-induced multiple PT-symmetry breaking transitions and reentrant localization transitions in nonHermitian Floquet quasicrystals. Phys Rev B 2022;106(5):054307.
[38] Chami N, Arbouche O, Chibani S, Driss Khodja FZ, Amara K, Ameri M, et al. Computational prediction of structural, electronic, elastic, and thermoelectric properties of FeVX (X= As, P) half-Heusler compounds. J Electron Mater 2020;49(8):4916–22.
[39] Xi L, Yang J, Wu L, Yang J, Zhang W. Band engineering and rational design of high-performance thermoelectric materials by first-principles. J Materiomics 2016;2(2):114–30.
[40] Drici L, Belkharroubi F, Boufadi FZ, Ameri I, Ameri M, Belkilali W, et al. First-principles calculations of structural, elastic, electronic, and optical properties of CaYP (Y= Cu, Ag) Heusler alloys. Emergent Mater 2022;5(4):10391054.
[41] Ameri M, Bennar F, Amel S, Ameri I, Al-Douri Y, Varshney D. Structural, elastic, thermodynamic and electronic properties of LuX (X= N, Bi and Sb) compounds: first principles calculations. Phase Transit 2016;89(12):1236–52.
[42] Mentefa A, Boufadi FZ, Ameri M, Gaid F, Bellagoun L, Odeh AA, et al. First-principles calculations to investigate structural, electronic, elastic, magnetic, and thermodynamic properties of full-heusler Rh2MnZ (Z= Zr, Hf). J Supercond Nov Magn 2021;34(1):269–83.
[43] Asma B, Belkharroubi F, Ibrahim A, Lamia B, Mohammed A, Belkilali W, et al. Structural, mechanical, magnetic, electronic, and thermal investigations of Ag2YB (Y= Nd, Sm, Gd) full-Heusler alloys. Emergent Mater 2021;4(6):1769–83.
[44] Benaddi F, Belkharroubi F, Ramdani N, Ameri M, Haouari S, Ameri I, et al. Electronic and magnetic investigation of half-metallic ferrimagnetic full-Heusler Mn2IrGe. Emergent Mater 2021;4(6):1745–60.

[45] Moussali A, Amina MB, Fassi B, Ameri I, Ameri M, AlDouri Y. First-principles calculations to investigate structural and thermodynamic properties of Ni2LaZ (Z= As, Sb and Bi) Heusler alloys. Indian J Phys 2020;94(11):1733–47.
[46] Matar SF, Solozhenko VL. Novel ultra-hard hexacarbon allotropes from first principles. Solid State Sci 2022:106884.
[47] Dulong, P.L. and Petit, A.T., 1819. Recherches sur quelques points importans de la theorie de la chaleur.
[48] Khireddine A, Bouhemadou A, Alnujaim S, Guechi N, Bin-Omran S, Al-Douri Y, et al. First-principles predictions of the structural, electronic, optical and elastic properties of the zintl-phases AE3GaAs3 (AE= Sr, Ba). Solid State Sci 2021;114:106563.
[49] Fadila B, Ameri M, Bensaid D, Noureddine M, Ameri I, Mesbah S, et al. Structural, magnetic, electronic and mechanical properties of full-Heusler alloys Co2YAl (Y= Fe, Ti): first principles calculations with different exchange-correlation potentials. J Magn Magn Mater 2018;448:208–20.
[50] Ayad M, Belkharroubi F, Boufadi FZ, Khorsi M, Zoubir MK, Ameri M, et al. First-principles calculations to investigate magnetic and thermodynamic properties of new multifunctional full-Heusler alloy Co2TaGa. Indian J Phys 2020;94(6):767–77.
[51] Li C, Wang Z, 2012. Computational modelling and ab initio calculations in MAX phases–I. Advances in Science and Technology of Mn+ 1AXn Phases, pp.197-222.
[52] Clarke DR. Materials selection guidelines for low thermal conductivity thermal barrier coatings. Surf Coat Technol 2003;163:67–74.
[53] Fine ME, Brown LD, Marcus HL. Elastic constants versus melting temperature in metals. Scr Metall 1984;18:951–6.